Experimental and numerical analysis of Carbon Fiber Reinforced Polymer notched coupons under tensile loading

Joël Serra, Christophe Bouvet, Bruno Castanié, Caroline Petiot

Experimental and numerical analysis of Carbon Fiber Reinforced Polymer notched coupons under tensile loading

Joël Serra [a], Christophe Bouvet [a,*], Bruno Castanié [a], Caroline Petiot [b]

[a] Université de Toulouse – Institut Clément Ader (UMR CNRS 5312) – INSA, ISAE-Supaéro, Mines Albi, UPS, Toulouse, France
[b] Airbus Group Innovations – 12 rue Pasteur, 92152 Suresnes, France

Keywords:
Infrared thermography
Notched tensile test
Discrete Ply Modeling
Experiments
Finite element model

A B S T R A C T

The behavior of composite laminates subject to notch based stress concentrations is difficult to apprehend, especially the mechanisms of damage progression leading to total failure. Numerical and experimental investigations were carried out on three different stacking sequences of notched, thin ply carbon/epoxy laminates. This paper presents a computational study of notched tensile tests (U-notch) using the Discrete Ply Modeling (DPM) method, which has already proved efficient on both in-plane and out-of-plane loading cases, such as pull through, low velocity impact and compression after impact. The specificities of this finite element model are its discrete nature (interface elements to model delamination and matrix cracks), the small number of parameters required, and its robustness. This work follows on from the study of open-hole tensile tests (same three layups) by the same authors [1] and analyzes the influence of layup and notch shape. Comparisons with experiments (using infrared technology) demonstrate that tensile strengths, and failure scenarios and patterns are predicted with acceptable accuracy.

1. Introduction

Composite materials are now largely used in most transport vehicles, especially in the aerospace and astronautics fields [2]. To demonstrate the strength of a fuselage, aircraft manufacturers must prove that it can sustain extensive damage called a "2-bay crack" (Fig. 1). Thus notched strength is one of the main design drivers for aeronautic composite structures. In order to evaluate the residual strength of composite structures with a hole or notch, two main types of method can be used; stress-based methods and energy-based methods.

1.1. Literature review

The stress-based methods use the stress field in the vicinity of the hole/notch and the energy-based methods use the evolution of the Strain Energy Release Rate (SERR) when the crack propagates. For example, a stress-based method, the well-known "point stress" failure model [4,5] uses the stress at a distance d_0 from the hole/notch in order to apply a failure criterion and to evaluate the structure failure. The physical meaning of this distance d_0 is the damaged area at the hole/notch tip that smooths the stress field. A similar distance is used in the "average stress" failure model [4,5]. For this model, the stress is averaged over a distance d_0, called the "average distance", in order to smooth the stress field calculated in the neighborhood of the hole/notch. This distance d_0 allows simple elastic Finite Element (FE) calculations to be used, and avoids the need for complex calculations taking the composite damage into account. These methods also make it possible to simulate the size effect [6–10], even though d_0 can depend on several factors [11], such as the stacking sequence, material, hole/notch size, etc. In particular, the size effect leads to the result that a small hole is less penalizing than a large hole (for homothetic size of structures). If the average distance is taken to be constant, d_0 will be proportionally greater for a small hole than for a large one.

Numerous experiments have been conducted to explore the physical meaning of the size effect [6–10]. For example, Wisnom et al. [8] studied the size effect on isotropic specimens with thin plies. They showed that the strength of notched composite laminates decreased when the notch size increased and concluded that the hole size effect was triggered by the presence of non-critical damage at the ply level, such as fiber failure, ply splitting, delamination or matrix cracking in the vicinity of the hole, which smooths the stress concentration. The ratio of the size of this "fracture process zone" to the specimen size explains the strength difference between small and large specimens.

* Corresponding author.
E-mail address: christophe.bouvet@isae.fr (C. Bouvet).

http://dx.doi.org/10.1016/j.compstruct.2017.08.090

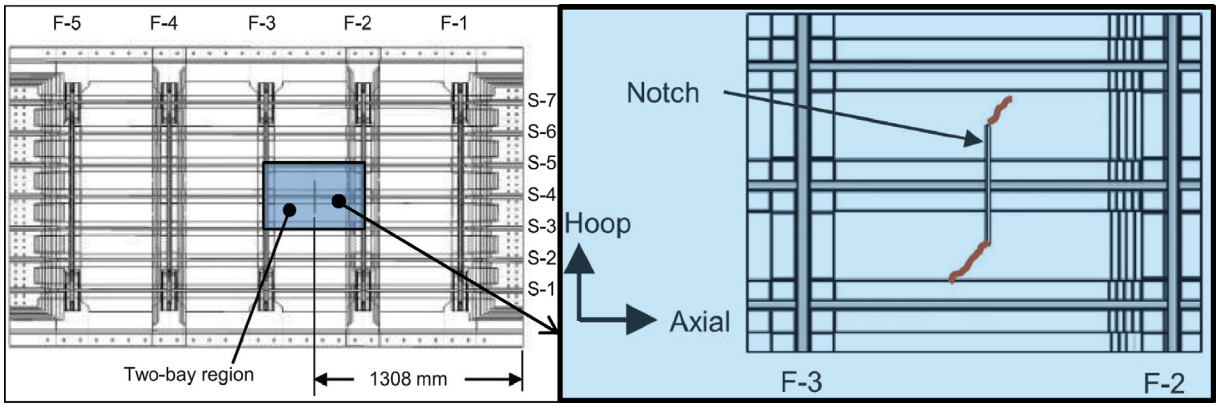

Fig. 1. Location of the "2-bay crack" in the fuselage [3].

Energy-based methods use the SERR (or the strain intensity factor) at the crack vicinity in order to evaluate whether the crack propagates and whether the propagation is stable [12]. The same concept of average distance can also be used to take account of the damage developing at the crack tip without performing complex calculations involving the composite damage [13–15].

A lot of models in the literature are based on stress-based methods and energy-based methods with an average distance concept [4,5,11,16–21]. However, it can be difficult to assess whether a stress-based method or an energy-based method is more suitable to evaluate the residual strength of a given holed/notched composite structure. In addition, the average distance (d_0) is often difficult to evaluate and can change with the structure size. Eventually, it is necessary to develop models able to evaluate the residual strength whatever the size and the shape of the hole/notch. Camanho et al. proposed an alternative approach to evaluate the residual strength of composite laminates with a hole or crack [10]. This analytical approach relies on a both stress- and energy-based method. This theory, initially introduced by Leguillon [22], predicts failure when both criteria are met. Compared to classic stress-based or energy-based methods, the main interest of this approach is to evaluate the failure strength of the structure and the average distance at the same time, avoiding having to choose the average distance *a priori*. In the same way, Y. Mohammed et al. used cohesive laws [23] to determine the strength of an open-hole composite laminate sample. This model, based on Dugdale's [24] and Barenblatt's [25] cohesive law concept links the failure strength to the length of the process zone.

These fast analytical and numerical methods are very useful and easy to use but often do not take the influence of the stacking sequence into account since the strain field is assumed to be constant within the laminate thickness (due to the plate model) [26]. However, experimental results show substantial influence of the stacking sequence on both failure scenarios and strengths [27,28]. For example, the final failure of composite laminates with thick plies is mainly driven by delamination propagation [8,29]. This stacking sequence effect was also observed in the present study, where the failure strength of plain specimens was observed to vary by about 30% between the different stacking sequences of laminates with the same number of plies in each direction (Table 2).

Moreover, more complete numerical models are needed to consider the damage (delamination, matrix cracking, fiber failure, etc.) developing in the vicinity of the hole/notch and to predict the final failure strength. Many models have been proposed in the literature [1,4,10,11,15,29–37] to simulate damage and to predict final failure in composite structures. The 3 main types of damage (fiber failure, matrix cracking and delamination) must be taken into account in order to accurately simulate damage in composite laminates and, in particular, to simulate the process zone in the vicinity of the hole/notch. For example, Camanho et al. [26] developed a model, based on continuum damage mechanics, able to simulate the onset and propagation of the main damage types. Abisset et al. used the damage meso-model [32] to model diffuse damage and matrix cracking with a progressive damage law, whereas a fracture mechanics law was used for fiber failure [38]. The failure modes of a notched specimen subjected to tensile loading were predicted with good accuracy, but a large number of parameters was needed, which could be difficult to evaluate. Cohesive interface elements are also often used to simulate delamination, and sometimes matrix cracking. For example, Pinho et al. developed a model able to predict fiber and matrix cracking using smeared crack models and delamination using interface elements [39,40]. ONERA is developing a model based on a multi-scale progressive failure approach, to describe the softening behavior of the fiber failure, and interface elements, to account for delamination [41]. Similarly, Ridha et al. built a progressive damage model based on the different damage mechanisms [42], in which continuum damage mechanics is used to represent the in-plane damage and cohesive elements for delamination. Cohesive interface elements are also sometimes used to represent matrix cracking. For example, Wisnom et al. used Weibull's approach to represent fiber failure, cohesive interface elements to model delamination, and other interface elements inside plies to model splitting at the edge of

Table 1
Test matrix.

Layups	C3-1	C3-2	C3-3
Coupon number	1, 2, 3, 4	5, 6, 7	8, 9, 10, 11
IRT Camera	Close-up (1, 2, 3) Wide shot (4)	Close-up (6) Wide shot (5)	Close-up (8, 9) Wide shot (10, 11)
DIC cameras	Close-up (4) Wide shot (1, 2, 3)	Close-up (5) Wide shot (6, 7)	Close-up (10, 11) Wide shot (8)

Table 2
Results of plain, open-hole and notched tensile tests.

Specimens	C3-1		C3-2		C3-3	
	$\overline{\sigma}^{\infty}$(%)	CV (%)	$\overline{\sigma}^{\infty}$(%)	CV (%)	$\overline{\sigma}^{\infty}$(%)	CV (%)
"Plain"	81	2.5	79	3.7	99	1.5
"Small"	61	4.4	58	1.6	71	9.4
"Medium"	56	1.7	54	4.5	67	0.7
"Large"	53	0.5	50	1.3	57	4.1
"Notched"	**38**	**2.5**	**41**	**5.0**	**40**	**1.7**

the hole [43–45]. This work raises the question of whether there is a need for cohesive interface elements to accurately simulate matrix cracking and its interaction with delamination [45]. The Discrete Ply Model (DPM), used in this paper, was one of the first models to use cohesive interface elements to simulate matrix cracking and delamination [46,47]. Other models of the same type exist in the literature [3,8,48–50].

1.2. Purpose of the study

The objective of this paper is to show that it is possible to simulate two very different tests including stress concentrations using the same model. The first analysis deals with the open hole tensile test and the scaling effect. This work was presented in a previous paper [1] and showed that the DPM was able to simulate the open hole tensile test with 3 different hole diameters (1 mm, 3.175 mm and 6.35 mm). The failure of this test is clearly a stress-based failure, driven by the stress field in the vicinity of the hole and by the average distance d_0. The scaling effect observed in this case can be seen as an interaction of the process zone with the hole size. The higher the ratio of the average distance d_0 to the hole diameter is, the more important is the smoothing of the stress around the notch and the higher is the failure strength. In order to simulate this test and to obtain the size effect numerically, it is necessary to simulate damage of different types, such as matrix cracking, delamination or fiber breakage, and the interaction between these different types of damage is of great importance if the process zone is to be simulated accurately.

The second analysis, which is the topic of the present paper, deals with the notch tensile test. It is the goal of the present work to study the development of damage during a notch tensile test and to compare it with that found in the open hole tensile test. The challenge is both experimental and numerical. Experimentally, it concerns following the crack propagation during the test. Infra-Red Thermography (IRT) was used for this purpose and showed very interesting results. Numerically, the challenge is to use the DPM to simulate a stress-based test (the open hole tensile test) and an energy-based test (the notch tensile test). In order to simulate these different tests, it is necessary to take the process zone, and in particular matrix cracking, delamination and their interaction, into account. It is of equal importance to take the crack propagation into account, and in particular the energy dissipated by the tensile fiber failure.

1.3. Analytical results

"U-notch" specimen failure is clearly energy-based failure that is driven, to a first approximation, by the evolution of the SERR when the crack propagates. The problem is not trivial and a process zone is created in front of the notch at the beginning of the test and also in front of the crack initiated from this notch propagation during the test. In the present case, the propagation is stable during the first part of the experiment. The stability of the crack propagation is classically driven by the evolution of the SERR with the crack length: if the curve is increasing, the propagation is unstable and, if the curve is decreasing, the propagation is stable. Nevertheless, this stability criterion should be considered with caution, because it is true only if the SERR curve versus the crack length is accurate. This curve can be difficult to evaluate because the process zone smooths the stress at the crack tip; it moves with the crack propagation and its size and morphology can change. The creation of the process zone explains the dissipation of energy during the crack propagation and the evolution of its size explains the R-curve: the farther the crack propagates, the larger is the size of the process zone, the higher is the energy needed to propagate the crack and the higher is the critical SERR.

In order to highlight the failure scenario of the 2 test types studied here, the open hole and the notched tensile test, the curves of the SERR (in the framework of linear fracture mechanics) are plotted versus the crack length in Fig. 1. These curves, and the physical meaning extracted from them, should be taken with caution because they were elaborated with a simple elastic FE calculation with plate theory and the process zone was not simulated.

It is very important to note that, in this figure, we chose to plot the SERR for the failure stress of each test. Different values of failure stress were obtained for the 4 experiments: 0.63 (dimensionless stress) for the 1 mm-diameter hole, 0.59 for the 3.175 mm-diameter hole, 0.53 for the 6.35 mm-diameter hole and 0.4 for the notched specimen (these stresses were evaluated as the average of the failure stress for the 3 stacking sequences given in Table 2). This choice made it possible to highlight whether the final failure was more stress-based or energy-based. It is clear in this figure that the SERR of the open hole tensile test was very low, and thus the final failure should be stress-based, while the SERR of the notched tensile test was near the fracture toughness of tensile fiber failure, and thus the final failure should be energy-based. Nevertheless, the fracture toughness of tensile fiber failure is difficult to evaluate and a few values are available in the literature. We considered about 80–100 N/mm for this type of material [51,52].

A few additional remarks may help with the interpretation of the curves of the open hole specimens. The curve of the 1 mm-diameter hole tends towards high values when the crack length tends to 2 mm. This is, of course, because the width to diameter ratio equals 5, so the ligament size equals 2 mm. Similar results were obtained at 6.35 mm for the 3.175 mm-diameter hole and at 12.7 mm for the 6.35 mm-diameter hole. The SERR curves of the holed specimens are strongly increasing and explain why the final failure scenario of these tests is unstable and brutal. This brutal final failure was obtained experimentally, except for 2 samples of 6.35 mm-diameter, where IRT showed the propagation of a small, stable crack. These experimental results should be taken with caution because it is more difficult to observe crack propagation in small specimens than in large ones.

The curves of the 3 hole sizes (Fig. 2) also explain why small specimens are more resistant than larger ones. Furthermore it should be kept in mind that, to evaluate the failure using these curves, an average distance d_0 should be used and a value of d_0 of about 1 mm would be appropriate as a first approximation [4,5]. The difference between the SERR curves should be assessed bearing in mind that the failure stress was used for the FE calculations. Then, as the failure stress is higher for the small hole than for the medium sized one, the SERR curve of the small hole would have been lower if the calculation had been made with the failure stress of the 3.175 mm-diameter hole (the SERR varies as the square of the stress). A comparison of the SERR curves of the 3 holes with different diameters for a given stress could clearly explain the hierarchy of the failure stress, except that the failure is stress-based and not energy-based! Consequently, the curve of the SERR should not be used to evaluate the failure strength but the stress field should be used. (It gives similar conclusions.)

The open hole tensile test is, however, not the topic of this paper and this article focuses on analyzing notched specimens. The SERR curve provides us with very interesting information. This curve is strongly increasing for the first 0.4 mm of crack length and becomes flatter thereafter (Fig. 2). This strong increase is, of course, linked to the notch end radius, which was equal to 0.5 mm in this study. The SERR curve of a perfect crack was plotted for comparison and the 2 curves are very similar as the crack length is more than 0.5 mm. This result highlights why no significant influence of the notch end radius is found experimentally, if the radius is small enough. After this first strong increase, the SERR increases more gradually. In fact, during the experiment, the crack propaga-

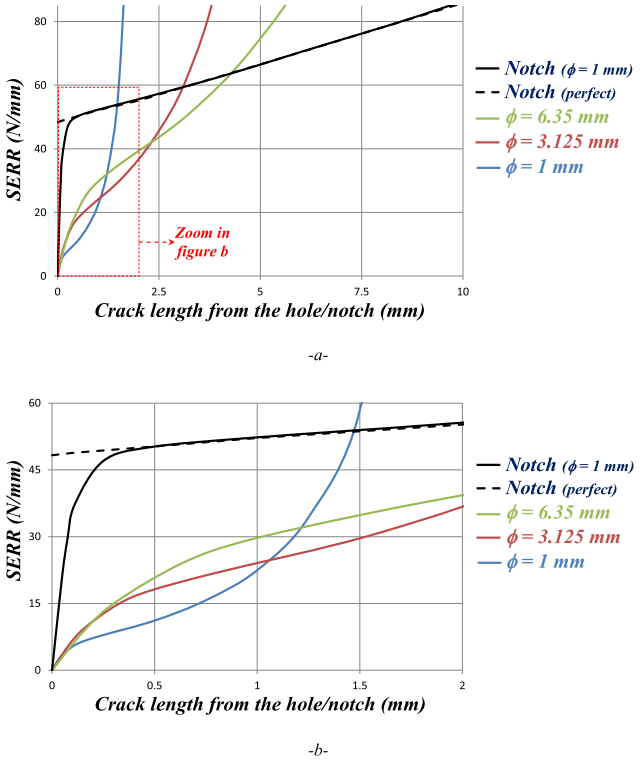

Fig. 2. SERR versus crack length for holed and notched specimens (a) and zoom on the first 2 mm (b).

tion was stable up to a crack length of about 10 mm. This result is not surprising seeing the SERR curve, considering that this curve should be taken with caution because the FE calculation is elastic and the process zone is not taken into account (and should induce an R-curve effect).

2. Experimental work

2.1. Material and setup

The material investigated in the present study was Hexcel's T700-M21 carbon epoxy unidirectional laminate with a nominal ply thickness of 0.125 mm. Three symmetric stacking sequences of 13 plies were studied. They presented the same number of plies in each direction (0°, 90° and ±45°), and only the relative position of plies changed between layups:

- C3-1 [45/-45/X/X/X/90/0/90/X/X/X/-45/45]
- C3-2 [X/X/X/X/0/90/0/90/0/X/X/X/X]
- C3-3 [X/X/X/X/X/0/0/0/X/X/X/X/X]

For confidentiality reasons, the draping sequences cannot be fully disclosed in this article. The sample studied was 180 mm wide and 300 mm long (not taking the grips into account) with a 30 mm central notch having an end notch radius of 0.5 mm (Fig. 3). The ratio of sample width to notch length was 6, so slightly higher than for holed specimens (W/D = 5), and the SERR curve was clearly higher because of this ratio and the notch shape (Fig. 2).

Tests were performed at ambient temperature (about 20 °C) using a 450 kN hydraulic machine at a displacement control speed of 0.02 mm/s. During the test, displacement was measured using an LVDT sensor and load was measured using the load machine's sensor. Two stereo-correlation cameras were also positioned on one side of the specimen and an IRT camera on the other side

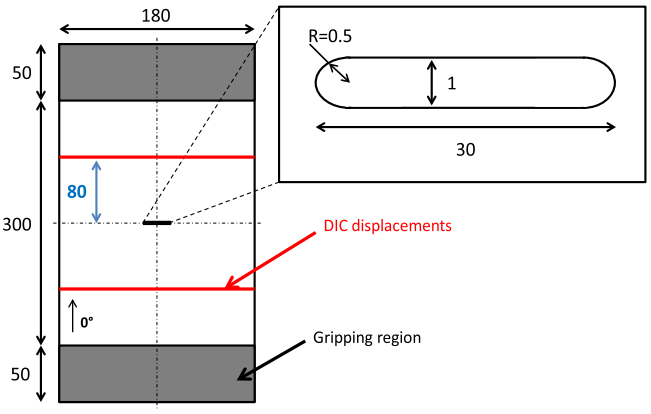

Fig. 3. Notched specimen geometry (dimensions in mm).

(Fig. 4). Images were analyzed with VIC 3D for the stereo-correlation and Altair® for the IRT measurements. Unfortunately, the coupons slipped in the machine grips during the tests, so the strains shown in this paper were evaluated using displacement from Digital Image Correlation (DIC) measures over a distance of 160 mm (Fig. 3).

Four specimens were tested to total failure for the C3-1 and C3-3 layups, and three for C3-2. Different configurations linked to the camera lenses (close-up/wide shot, summarized in Table 1), were used in order to obtain the maximum amount of information on the fracture scenario. Stress/strain curves (Fig. 6) were consequently derived from configurations in which the DIC cameras displayed a large part of the specimen (wide shot). For close-up configurations, only failure loads were determined and are schematized with arrows in Fig. 5. Experimental setup errors on DIC camera parameters for specimen n°9 and on the IRT camera parameters for specimen n°7 made it impossible to use these images.

2.2. Results

Similarly to the experimental results obtained in the previous study of open hole tension tests [1], the present experimental results (Table 2) showed little discrepancy for the three stacking sequences. In Table 2, "Plain" refers to plain samples used to compare results with holed/notched samples, "Small" refers to the 1 mm-diameter hole, "Medium" to the 3.175 mm-diameter hole, "Large" to the 6.35 mm-diameter hole, "Notched" to the notched samples, $\overline{\sigma}^{\infty}$ to the mean remote failure stress and CV to the coefficient of variation. To respect privacy policy, the level of stress and strain was normalized by the maximum failure stress reached by one coupon of the C3-3 layup. On average, C3-2 and C3-3 layups exhibited a total failure load slightly larger than that of the C3-1 layup. Differences between stacking sequences were much reduced compared to plain and open-hole tension tests. In comparison with holed specimen tests, failure loads were much lower. No structural failure (B) – defined as the first occurrence of load or stiffness dropping by more than 5% – was detected before total failure, except in coupons n°1 and n°8.

2.2.1. Oriented laminate C3-1

2.2.1.1. Failure scenarios and patterns. The first damage observed on the C3-1 layup from point A (Fig. 5) could be fiber/matrix debonding, matrix cracking, delamination or fiber breakage. The most energetic failure mode is fiber fracture. A local increase in temperature of about one degree (Fig. 6) seems to indicate such a failure mode [53]. The others are less energetic: they increase the temperature locally by a few tenths of a degree [53,54].

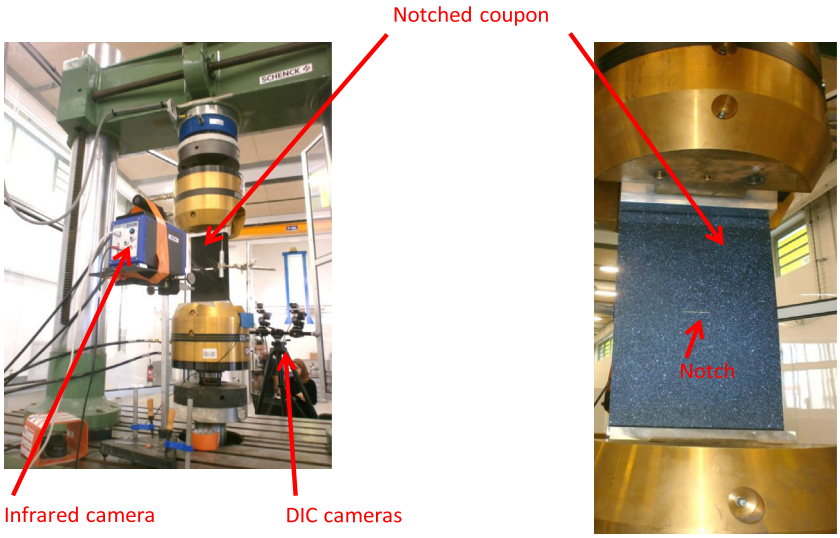

Fig. 4. Experimental setup for the notched quasi-static tension test.

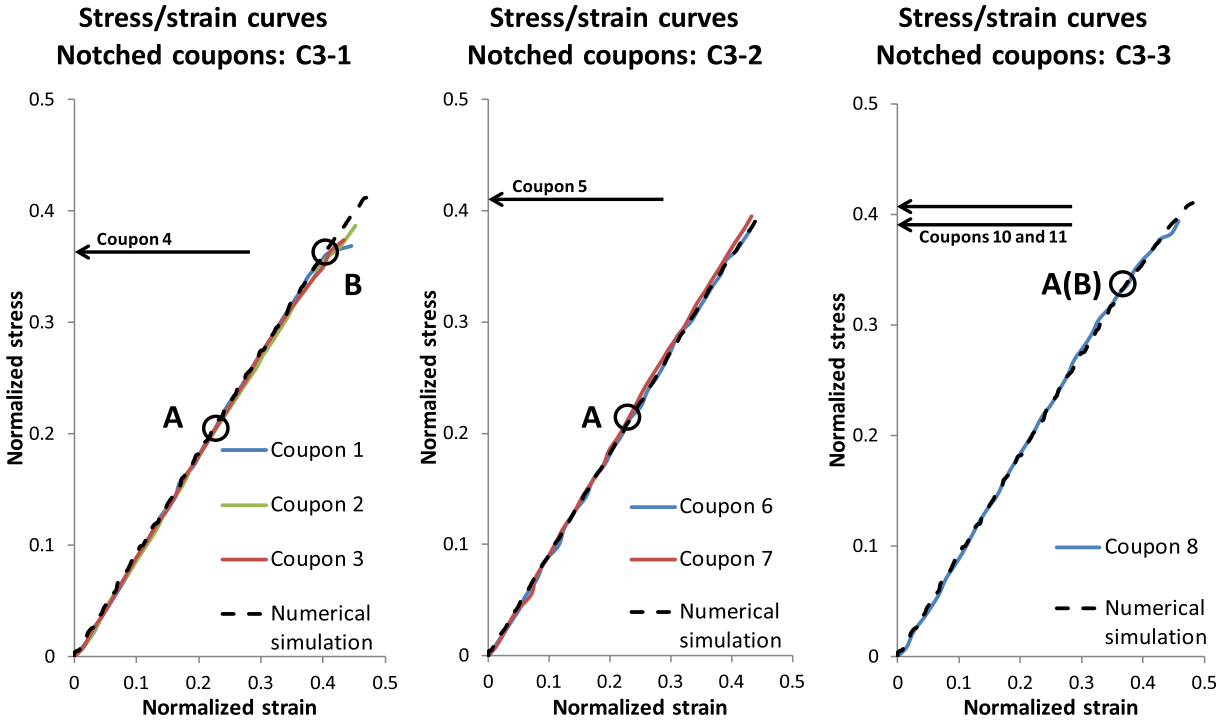

A, *First damage detected with the use of the infrared technology*
B, *Structural failure*

Fig. 5. Stress/strain curves of the three notched layups (C3-1, C3-2 and C3-3) – comparison between numerical and experimental data.

Once the propagation had begun, emissions of heat were detected on the right side of the notch (close-up for coupons n° 1, 2 and 3, Fig. 6). They appeared to be relatively symmetrical on either side of the notch (wide shot for coupon n°4, Fig. 6). The damage then continued to progress up to a brutal total failure. The crack propagated in an explosive manner, oriented at a few degrees with respect to the horizontal. After rupture of the laminate, a symmetrical pull-out failure pattern was obtained (Fig. 7).

2.2.1.2. Crack propagation. In order to allow the application of a new criterion for comparing the numerical results with the experimental results, two attempts were made to determine the evolution of the crack length during the test. The first used DIC, the second, IRT.

Using the DIC technique, we determined the longitudinal strain (ε_{yy}) field near the crack (Fig. 8) at different progressions of the tensile test (41, 43 and 45% in Fig. 9). Test progression ($\varepsilon_{average}$)was defined by the average strain of the specimen normalized by the maximum strain obtained (plain specimen of C3-3 layup). The longitudinal strain was compared with fiber failure strain (ε_0^T, Table 3) and, assuming the strain to be constant throughout the thickness of the laminate, it was possible to estimate the extent of broken fibers and then the crack length (along $\vec{x}$).

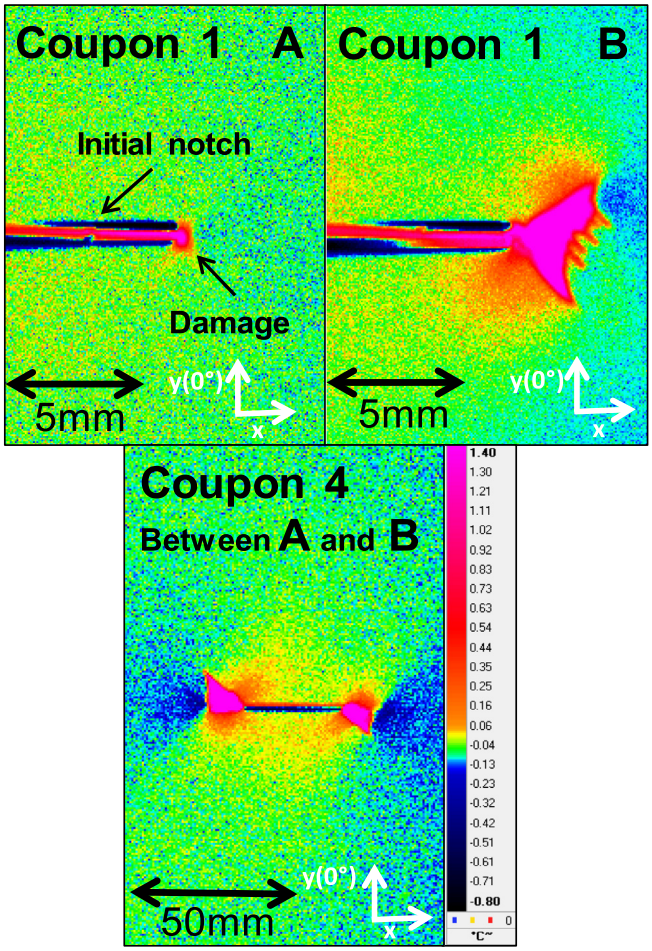

Fig. 6. Damage progression in coupon n°1 (wide shot) and n°4 (close-up) observed by IRT camera.

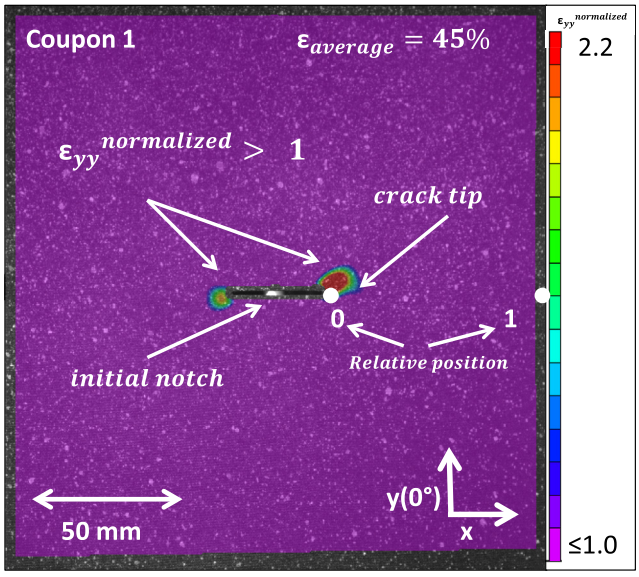

Fig. 8. Crack extension determined using DIC.

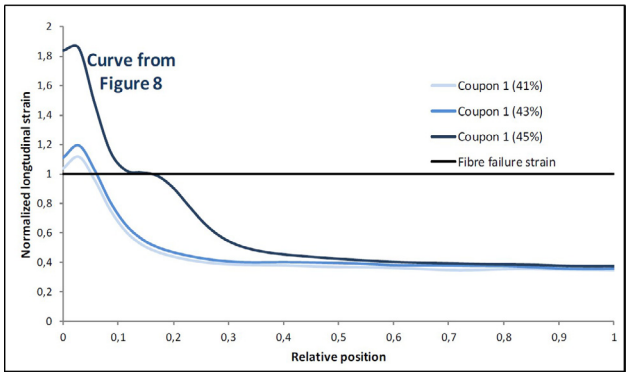

Fig. 9. Longitudinal strain measurement near the crack using DIC.

The relative position indicated (Figs. 9 and 10) is the position/length-of-ligament ratio; 0 corresponding to the notch edge and 1 to the free edge of the test coupon. Longitudinal strain (ε_{yy}) is normalized by the tensile fiber failure strain (ε_0^T) to become $\varepsilon_{yy}^{normalized}$ (Fig. 8). The purple area corresponds to strain ($\varepsilon_{yy}^{normalized}$) below 1, so, to a first approximation, to the zone without fiber fracture (in the y-direction).

It is then possible to obtain, from Fig. 8, the evolution of the fiber failure extent as a function of the normalized average strain ($\varepsilon_{average}$) enforced. This evolution is shown in Fig. 9. However, it is necessary to consider the evolution of the damage obtained with care since it was measured on the outside ply. Delamination between the various plies made it impossible to have a constant strain throughout the thickness of the laminate; a different strain of the 0° inside the thickness could be observed. Moreover, it is likely that the ply observed by the DIC cameras entered the inelas-

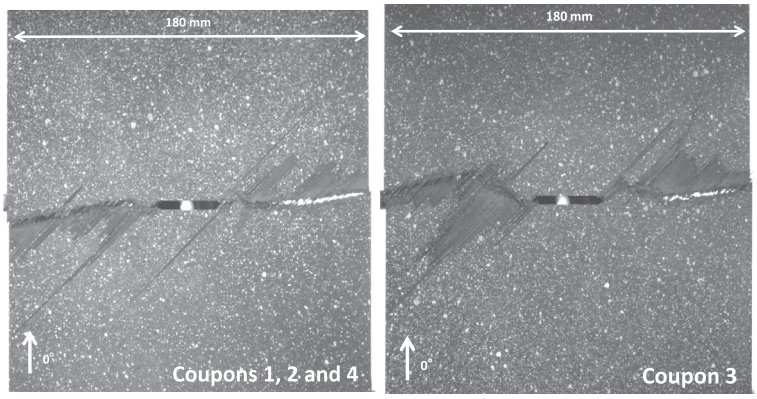

Fig. 7. Fracture facies of C3-1 layup.

Table 3
Material properties of the T700/M21 used in the Discrete Ply Model.

Elastic Properties		
E_1^T	Tensile Young's modulus in fiber direction	130 GPa
E_1^C	Compressive Young's modulus in fiber direction	100 GPa
E_2	Transverse Young's modulus	7.7 GPa
ν_{12}	Poisson ratio	0.3
G_{12}	Shear modulus	5.0 GPa
Matrix cracking		
Y^T	Transverse tensile strength	60 MPa
S^L	In-plane shear strength	110 MPa
Fiber failure		
ε_0^T (%)	Tensile strain in fiber direction at damage initiation	1.70%
ε_0^C (%)	Compressive strain in fiber direction at damage initiation	1.25%
$G_{Ic}^{fibre,t}$	Fracture toughness for mode I in tension	100 N/mm
$G_{Ic}^{fibre,c}$	Fracture toughness for mode I in compression	20 N/mm
Delamination		
G_{Ic}^{del}	Interface fracture toughness for opening mode (I)	0.5 N/mm
$G_{II,c}^{del}$	Interface fracture toughness for shear mode (II & III)	1.6 N/mm

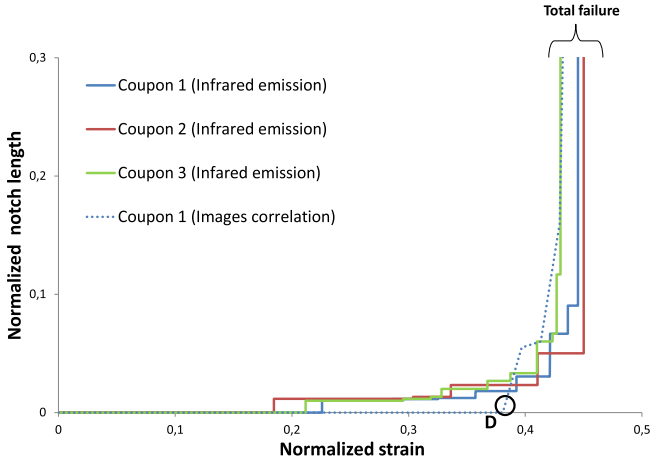

Fig. 10. Comparison of the two methods used to determine crack length evolution.

tic domain and, from then on, a measured strain greater than the tensile fiber failure strain does not necessarily denote fracture.

Composite laminates were then monitored with the help of an IRT camera in order to determine notch extension using a different methodology. Fiber rupture is very energetic compared to other types of damage but it was possible to track the crack progression by listing all the successive positions of heat emissions (Fig. 6). Thus the results given by the two methods could be compared (Fig. 10). IRT emission monitoring showed that damage occurred early in the test. In Fig. 10, D corresponds to the stage of the tensile test when the DIC showed a longitudinal strain (near the notch) greater than the fiber failure strain and therefore gives an estimation of the crack propagation extent. Before D, notch extension must be small; hence it is hidden inside the laminate with delamination around, which explains the absence of detection by DIC. After D, damage (fiber rupture, matrix cracking and delamination) becomes considerable at the notch edge and generates a longitudinal strain greater than the tensile fiber failure strain on the outside ply.

The notch extension determination method using IRT seems to be more relevant than the DIC process since the IRT does not assume a constant strain throughout the thickness of the laminate. However, it must slightly overestimate the crack progression due to the propagation of heat in the laminate. When a fiber from a 0° ply far from the outside surface breaks, the heat emitted propagates towards the surface until it is detected by the IRT camera. During this period of time, it also propagates within the plane of the laminate.

2.2.2. Oriented laminates C3-2 and C3-3

Failure scenarios associated with layups C3-2 and C3-3 were very similar to the ones observed for layup C3-1. In Fig. 5, from A, damage progresses from both notch ends and leads to total failure of the laminate.

The failure patterns shown in Figs. 11 and 12a reveal 45° oriented crack propagations ("Z shaped") for the two stacking sequences. Closer examination suggests that 0° fiber rupture has actually propagated along a direction approximately orthogonal to the tensile direction (Fig. 12b).

Afterwards, notch length evolutions (Figs. 13 and 14) were determined using the same IRT process as for C3-1 layup.

Crack propagation seems to initiate sooner for C3-1 layup than for C3-2 layup, and sooner for C3-2 layup than for C3-3 layup. Maximum stable crack propagation (just before brutal total failure) varies from 5% to 12% of the ligament (75 mm long) without significant differences between the three layups.

2.3. Conclusions drawn from the experiments

Regarding all tensile tests ("Plain", "Small", "Medium", "Large" and "Notched"), C3-3 layup appears to be the most resistant (it exhibits the highest failure stress, Fig. 15). Differences between layups are, however, reduced when failure stress decreases (edge effects become less critical).

Net failure stresses obtained for the "Notched" specimens are much smaller than open-hole ones (Fig. 15). This discrepancy is mainly related to the difference in SERR between notches and holes (Fig. 2).

In order to assess notch sensitivity independently of the stacking sequence effect (20% failure stress difference for "Plain" speci-

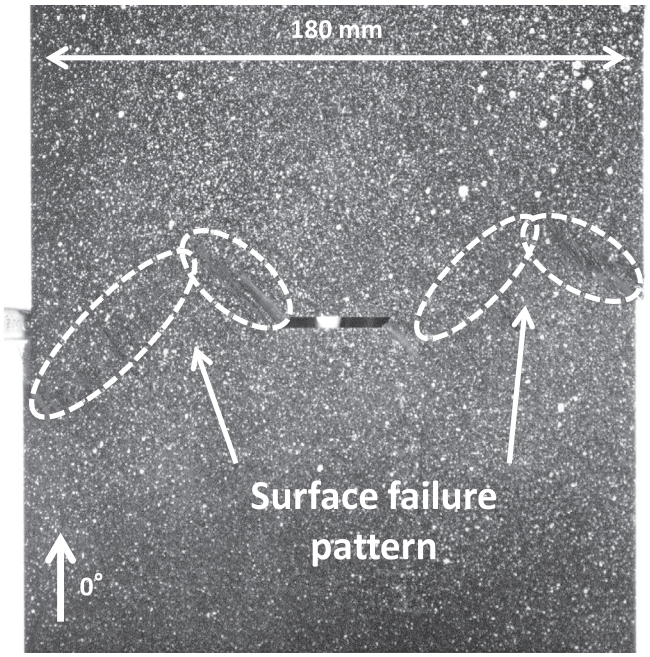

Fig. 11. C3-2 layup failure pattern.

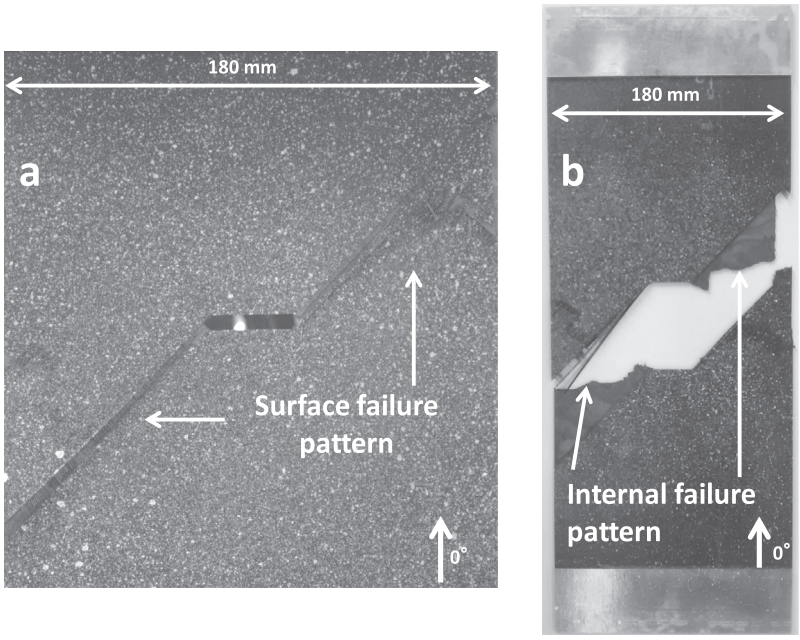

Fig. 12. C3-3 layup external (a) and internal (b) failure pattern.

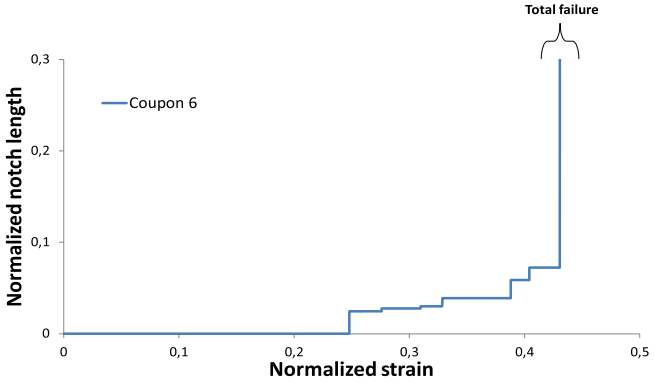

Fig. 13. Notch length evolution (C3-2 layup) based on IRT process.

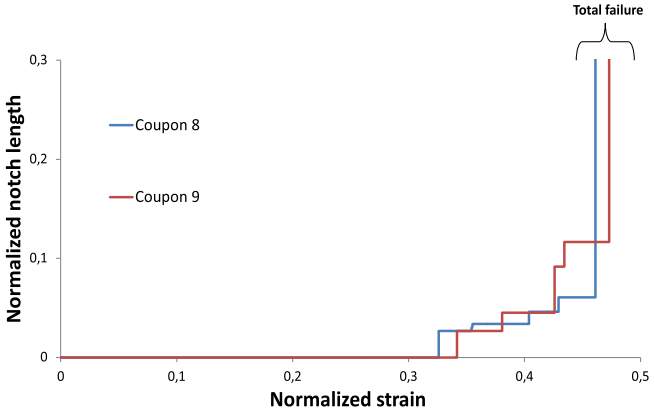

Fig. 14. Notch length evolution (C3-3 layup) based on IRT process.

mens), the failure stress of each configuration ("Small", "Medium", "Large" and "Notched") divided by "Plain" failure stress (for each layup) is summarized in Fig. 16. The layups C3-1 and C3-2 appear to be less sensitive to the presence of the cut than C3-3.

The justifications developed in [1] for the open-hole tension case seem to be valid here too. Edge effects, triggering delamination for "Plain" specimens observed under tension, have the opposite effect around a notch (they smooth stress concentration). C3-3 layup is not much subject to free edge delamination ("Plain" specimens). Hence it does not smooth stress concentrations near the notch and has a lower ratio (Fig. 16) than C3-1 and C3-2 layups.

3. Numerical modelling

3.1. DPM principle

The Discrete Ply Model has already been described in several papers [30,31,46,47] and the same characteristics were kept here as in [1] for scaled open-hole tension test modelling. The main features, such as mesh construction and behavior law, are briefly recalled below.

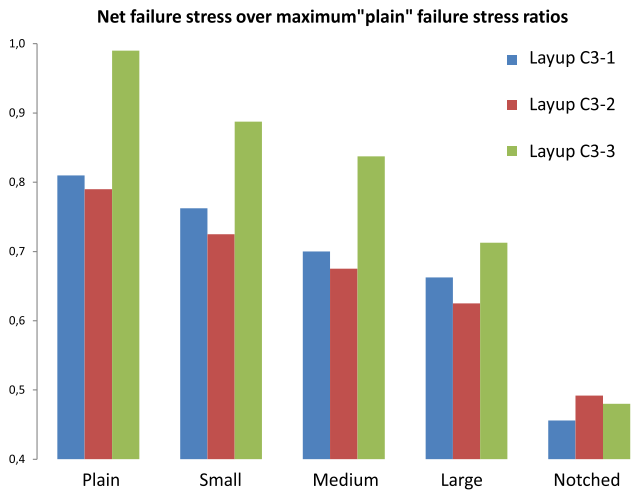

Fig. 15. Net failure stresses for all sizes and layups.

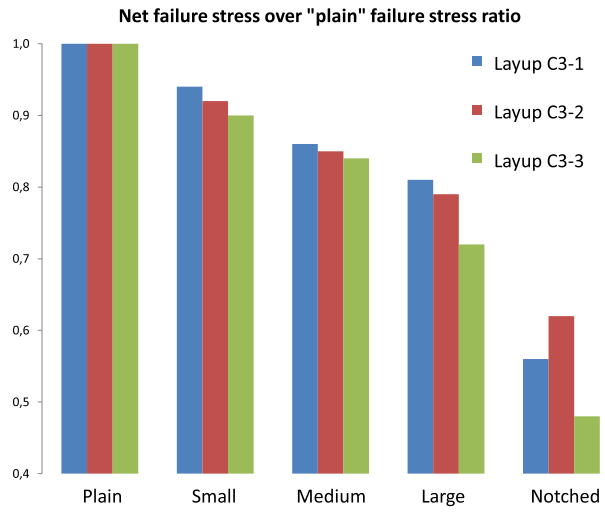

Fig. 16. Notch sensitivity for the three layups.

The principle of the DPM model is to simulate the major failure modes observed in composites as follows (Fig. 17):

- Delamination is taken into account using classical interface elements between two consecutive plies (or groups of plies) of different orientation, each ply being modeled with one volumic finite element in the thickness. Then, the damage in the delamination interface elements is classically driven by fracture mechanics.
- Matrix cracking is taken into account using interface elements normal to the transversal direction. The damage of the matrix cracking interface elements is driven using fracture criteria evaluated in the neighboring volumic finite elements. These interface elements induce complex meshing but make it possible to automatically simulate the interaction between intra- and inter-laminar damage. This interaction is crucial to account for the complex damage morphology observed in composite structures.

Fibre fracture is considered using continuum damage mechanics with an original formulation linking the integration points of the volumic finite element to impose a constant SERR per unit area [47]. This approach can be compared to methods using the characteristic element length which allows mesh-size-independent modelling [51,55,56]. First order volume elements (8 nodes per element) were selected in order to simulate bending phenomena correctly while using only one element per ply (thickness direction). Two nodes are sufficient to represent affine behavior within the element. Therefore the strain field within the laminate thickness is a piecewise defined function.

3.2. Meshing and calculation strategies

Applying a constant size mesh to the large dimension (180×300 mm^2) coupons would have generated prohibitive calculation costs. To solve this issue, different types of elements were used:

- The standard elements of the DPM elements, detailed in the previous paragraph (Fig. 17), for the zone near the notch (Fig. 18-zone 3)
- Volumic finite elements with reduced integration (and without interface elements) in zone 2 (Fig. 18-zone 2)
- Standard volumic elements with a homogenized laminate behavior far from the notch (Fig. 18-zone 1)

The last two types of elements, never damaged during the propagation of the crack emanating from the notch, made the calculation faster. Numerous iterations were necessary to estimate the three zone dimensions. The blue zone (3) was reduced as far as possible without disrupting notch propagation. Connection between zone 1 and zone 2 was realized through a kinematic coupling: nodes from plies at the border between zone 1 and 2 were constrained to follow the displacement of the corresponding zone 1 element face.

To further reduce calculation costs, planar and central symmetries were used. It was verified that modelling one fourth of the coupon gave results equivalent to when the whole specimen was meshed. To set planar symmetry corresponding to the laminate symmetry plane, since the three layups studied contained an odd number of plies, the middle ply was represented with a thickness of half a ply (0.0625 mm).

Since damage progression is substantial before total failure, a customized management of the distorted elements had to be implemented. First, the calculation was divided into two parts: one step including very little damage (corresponding to the part

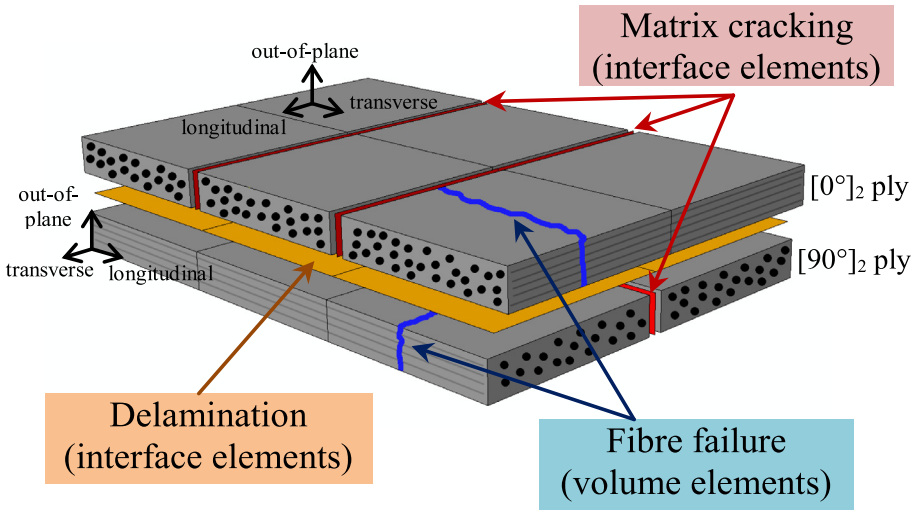

Fig. 17. Modelling of composite damage with the different element types [46].

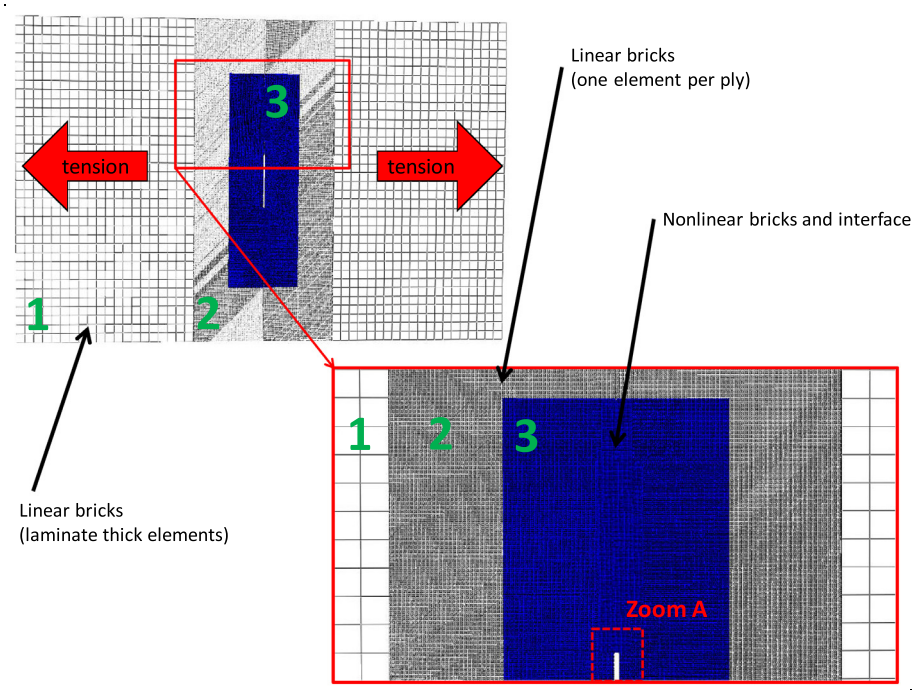

Fig. 18. Numerical model of a notch specimen under tensile stress.

of the stress/strain curve before A in Fig. 5) and the other from the initiation of damage propagation until total failure of the laminate. For the second part, the step time value was set to one third that of the first. The Abaqus "Distortion control" function was exploited to restrain the distortion of damaged elements through the use of an artificial energy. It was verified *a posteriori* that this energy was less than 1% of the internal energy. Even with those modifications, near the notch, element distortion (the first elements to be entirely damaged) made the calculation impossible. It was then decided to suppress totally failed elements, i.e. elements for which the associated energy was totally dissipated (fiber failure and delamination, cf. Fig. 17) or when the stress criterion was met (matrix cracking, cf. Fig. 17). The specimens being subject to tensile stress, deletion of these elements did not have any major influence (once "broken", elements do not withstand any load). It would not have been possible to draw this conclusion in a compression loading case (but distortion would not have been of the same magnitude).

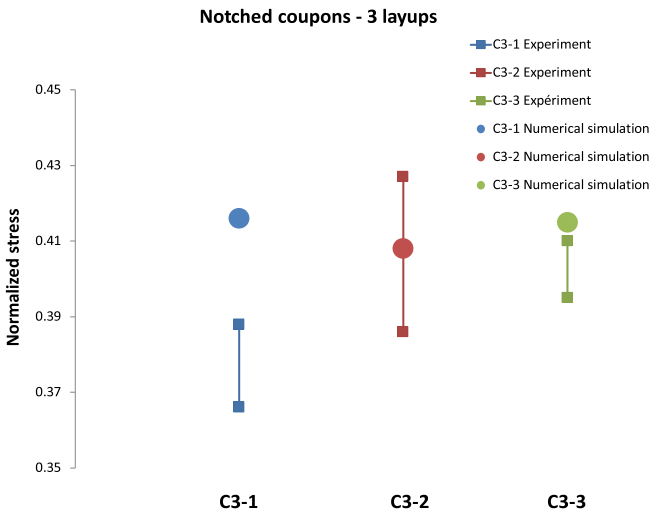

Fig. 19. Failure stress – numerical and experimental results.

Once all the necessary updates had been implemented, the calculation was run on 1.4×10^6 elements and lasted approximately 50 h (20 CPUs) using the EOS high performance calculator at CALMIP. The DPM uses a small number of parameters (Table 3), all of which were provided by experimental tests [1,30,46].

4. Model validation and discussion

Stress/strain curves obtained from numerical simulations correlated well with the experimental ones (Fig. 5). C3-3 layup stiffness loss (A-B) was well expressed by numerical simulation but failure stress relative order was not predicted correctly because failure

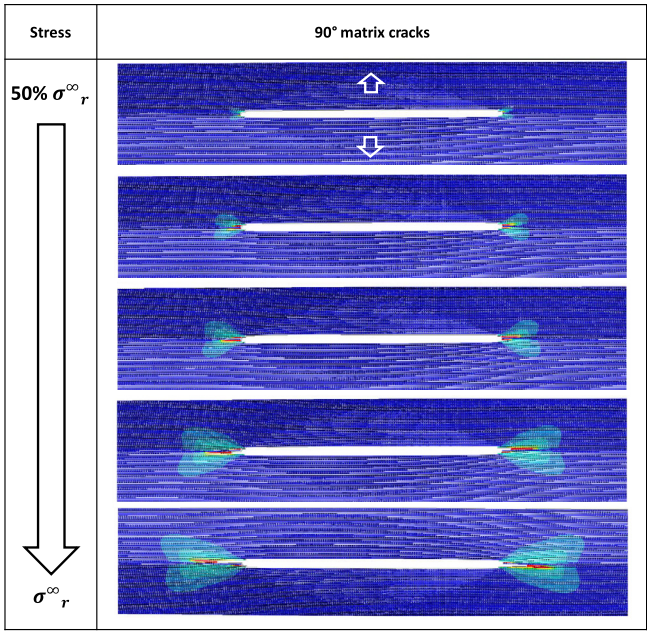

Fig. 20. Numerical simulation of 90° ply matrix cracking.

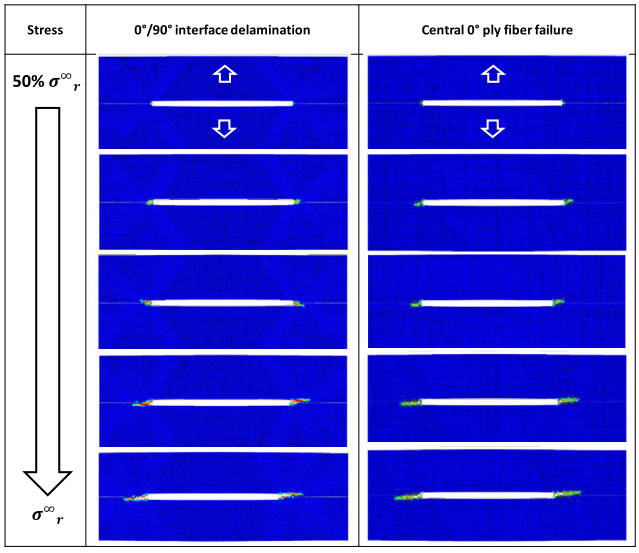

Fig. 21. Numerical simulations of 0°/90° interface delamination and central ply 0° fiber rupture evolutions.

stresses were slightly overestimated for C3-1 and C3-3 layups (Fig. 19). However, as experimental values were very close with non-negligible coefficients of variation (Table 2), reproducing this relative order was not of major importance.

The global behavior of laminates, represented by stress/strain curves, seemed to be correctly reproduced. To validate the numerical model further, notch evolution was determined for the three layups with the help of IRT technology (cf. § 2.2) and compared with simulations. Only the coupons shot in a close-up configuration (Table 1) were put to use. The others (wide-shot) did not enable a sufficiently precise length determination to be obtained. Numerical failure patterns were also compared to experimental ones.

4.1. Oriented laminate C3-1

Damage evolution of notched laminate was very progressive from A (Fig. 5). A "butterfly wings" type evolution of matrix cracking (Fig. 20) was obtained numerically (very similar to the one observed by [1,31] on open-hole tension configurations). The 0°/90° interface delamination and 0° fiber fracture seemed to propagate perpendicularly to the tensile direction until total failure (Fig. 21).

The numerical failure pattern of Fig. 22 is very similar to the experimental one. Notch propagation is limited by the dimensions of the damageable zone (zone 3, Fig. 18) but reached the free edge of the coupon during experimental tests.

The evolution of the C3-1 layup notch length determined by counting the numbers of completely damaged volume elements (central ply 0° fiber failure) in the numerical simulations was very consistent with that determined using IRT. Notch propagation initiation and its maximal amplitude before total failure (8% of the ligament), were predicted with good accuracy (Fig. 23).

4.2. C3-2 and C3-3 layups

Failure scenarios and patterns simulated with the help of the DPM for C3-2 and C3-3 layups were very similar to those obtained for layup C3-1. In consequence, the numerical model failed to reproduce the 45° external plies failure pattern ("Z shape", Figs. 11 and 12). Notch length evolutions were determined both numerically and experimentally (IRT) for C3-2 (Fig. 24) and C3-3 (Fig. 25) layups. The numerical model again predicted notch evolution kinematics that were very consistent with experiment.

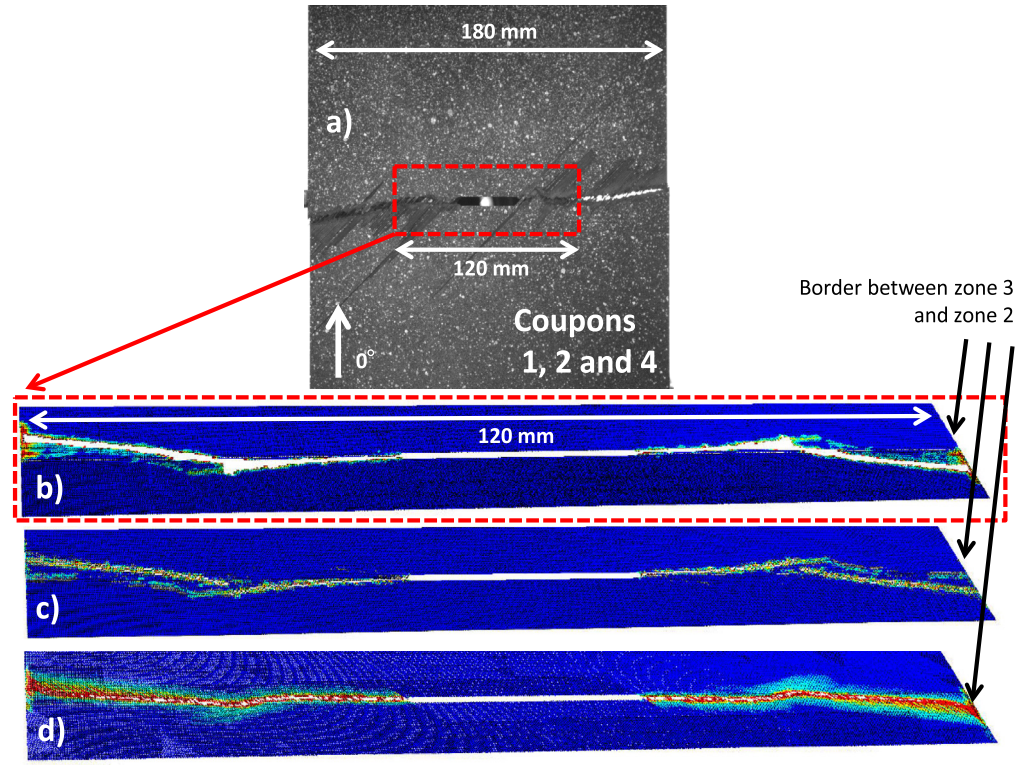

Fig. 22. C3-1 layup failure pattern comparison: a) Experimental, b) Central 0° ply fiber rupture, c) 45° outside ply matrix cracking, d) 0°/90° interface delamination.

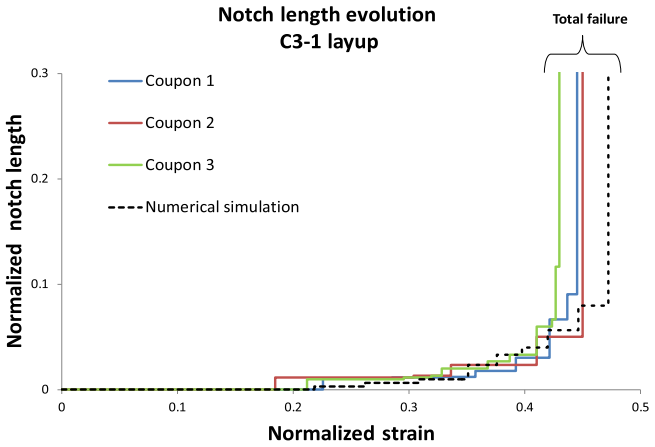

Fig. 23. Notch length evolution (C3-1 layup) – numerical and experimental results.

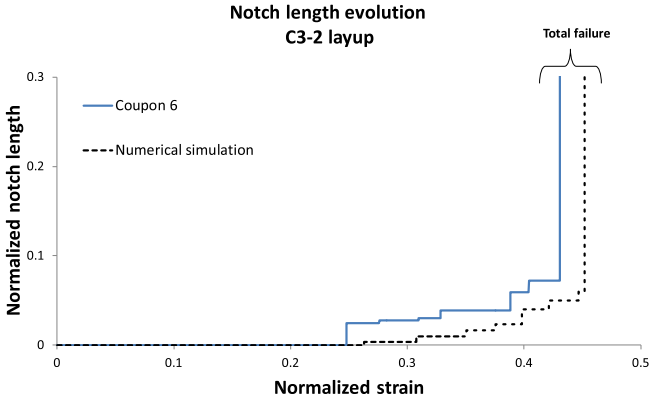

Fig. 24. Notch length evolution (C3-2 layup) – numerical and experimental results.

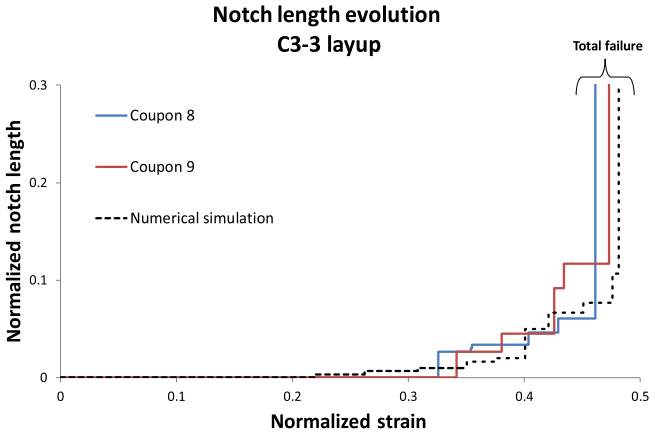

Fig. 25. Notch length evolution (C3-3 layup) – numerical and experimental results.

5. Conclusion

The purpose of the study described in this paper was to investigate the development of damage during a notched tensile test and to compare it with the open hole tensile test performed on the same three layups. Numerical results have been confronted with experimental data and the influence of both the notch shape and dimensions and the stacking sequence have been analyzed.

Notched tensile tests confirmed the tendency already observed on open-hole specimens [1]: even though the C3-3 layup was more sensitive to the presence of a cut than the other two (C3-1 and C3-2), it exhibited the highest failure stress. Strength differences (hole and U-notch) were related to the shape of the cut. The SERR at a U-notched edge is higher than in the vicinity of a cracked circular hole (Fig. 2). The failure of notched coupons is hence triggered earlier and propagates within the specimen (total failure) for a stress lower than that in open-hole coupons under tensile loading. Two methods were employed to record the behavior of notched coupons, DIC and IRT. Using IRT to determine the evolution of the notched length gave more accurate results than the process based on DIC.

Modifications of the numerical model were necessary to simulate notched coupons under tensile loading at a reasonable calculation cost. Simulation outputs were validated thanks to numerous experimental observations. The DPM thus proved its ability to simulate the behavior of notched (holes of different diameter and U-notch) coupons under tensile loading, then to simulate a stress-based test (the open hole tensile test) and an energy-based test (the notch tensile test). This shows that the approach is able to account for the process zone (in particular matrix cracking, delamination and their interaction) and to account for the crack propagation, (in particular the energy dissipated by the tensile fiber failure). Finally, in order to validate this numerical model at a higher level of the tests pyramid (structural level) and for different loading cases, a new test-rig, designed at the Institute Clement Ader, was used to test plates of large dimensions (400×400 mm^2) and the DPM was adapted to simulate these innovating structural tests.

Acknowledgements

The research that led to the results presented above received funds from the French National Research Agency under the VERTEX project MATETPRO program (ANR-12-RMNP-0001).

The academic authors gratefully acknowledge the support provided by Airbus Group Innovations. This work was granted access to the HPC resources of CALMIP under allocation 2012-P1026.

References

[1] Serra J, Bouvet C, Castanié B, Petiot C. Scaling effect in notched composites: the discrete ply model approach. Compos Struct 2016;148:127–43.
[2] Gay D. Composite materials: design and applications. 3rd ed. Taylor and Francis Group: CRC Press; 2015.
[3] Bergan A, Bakuckas J, Awerbuch J, Tan T-M. Assessment of damage containment features of a full-scale PRSEUS fuselage panel. Compos Struct 2014;113:174–85.
[4] Awerbuch J, Madhukar MS. Notched strength of composite laminates: predictions and experiments—a review. J Reinf Plast Compos 1985;4(1):3–159.
[5] Tan SC. Stress concentrations in laminated composites. Taylor and Francis Group: CRC Press; 1994.
[6] Bazant ZP. The scaling of structural strength. London: HPS; 2002 [1st publ.].
[7] Bazant ZP, Daniel IM, Li Z. Size effect and fracture characteristics of composite laminates. J Eng Mater Technol 1996;118(3):317–24.
[8] Wisnom MR, Hallett SR, Soutis C. Scaling effects in notched composites. J Compos Mat 2010;44(2):195–210.
[9] Xu X, Wisnom MR, Mahadik Y, Hallett SR. An experimental investigation into size effects in quasi-isotropic carbon/epoxy laminates with sharp and blunt notches. Compos Sci Technol 2014;100:220–7.
[10] Camanho PP, Maimí P, Dávila CG. Prediction of size effects in notched laminates using continuum damage mechanics. Compos Sci Technol 2007;67(13):2715–27.
[11] Kassapoglou C. Modeling the effect of damage in composite structures: simplified approaches. Wiley; 2015.
[12] Anderson TL. Fracture mechanics: fundamentals and applications. 3rd ed. CRC Press, Taylor and Francis Group; 2005.
[13] Kamala Kannan V, Murali V, Rajadurai A, Nageswara Rao B. Failure assessment on central-sharp notched carbon/epoxy laminates. Mat Design 2010;31(9):4348–55.
[14] Khashaba UA. Fracture Behavior of Woven Composites Containing Various Cracks Geometry. J Compos Mat 2003;37(1):5–20.
[15] Hochard C, Lahellec N, Bordreuil C. A ply scale non-local fibre rupture criterion for CFRP woven ply laminated structures. Compos Struct 2007;80(3):321–6.

[16] Waddoups ME, Eisenmann JR, Kaminski BE. Macroscopic fracture mechanics of advanced composite materials. J Compos Mat 1971;5:446–54.
[17] Yeh HY. Analytical damage zone size predictions for notched laminated composites. J Reinf Plast Compos 2004;23(18):2081–100.
[18] Zhen S. The D criterion theory in notched composite materials. J Reinf Plast Compos 1983;2(2):98–110.
[19] Chen P, Shen Z, Wang JY. Prediction of the strength of notched fiber-dominated composite laminates. Compos Sci Technol 2001;61(9):1311–21.
[20] Eriksson I, Aronsson CG. Strength of tensile loaded graphite/epoxy laminates containing cracks, open and filled holes. J Compos Mat 1990;24(5):456–82.
[21] Vieille B, Chabchoub M, Bouscarrat D, Keller C. Prediction of the notched strength of woven-ply PolyPhenylene Sulfide thermoplastic composites at a constant high temperature by a physically-based model. Compos Struct 2016;153:529–37.
[22] Leguillon D, Quesada D, Putot C, Martin E. Prediction of crack initiation at blunt notches and cavities – size effects. Eng Fract Mech 2007;74(15):2420–36.
[23] Mohammed Y, Hassan MK, El-Ainin HA, Hashem AM. Size effect analysis of open-hole glass fiber composite laminate using two-parameter cohesive laws. Acta Mech 2015;226(4):1027–44.
[24] Dugdale DS. Yielding of steel sheets containing slits. J Mech Phys Sol 1960;8 (2):100–4.
[25] Barenblatt GI. The mathematical theory of equilibrium cracks in brittle fracture. Adv Appl Mech 1962;7:55–129.
[26] Camanho PP, Hallett SR. Numerical modelling of failure in advanced composite materials. Woodhead Publishing; 2015.
[27] Hallett SR. Experimental investigation of progressive damage and the effect of layup in notched tensile tests. J Compos Mat 2005;40(2):119–41.
[28] Hessabi ZR, Majidi B, Aghazadeh J. Effects of stacking sequence on fracture mechanisms in quasi-isotropic carbon/epoxy laminates under tensile loading. Iran Polym J 2005;14(6):531.
[29] Wisnom MR. Modelling discrete failures in composites with interface elements. Compos A Appl Sci Manuf 2010;41(7):795–805.
[30] Adam L, Bouvet C, Castanié B, Daidié A, Bonhomme E. Discrete ply model of circular pull-through test of fasteners in laminates. Compos Struct 2012;94 (10):3082–91.
[31] Achard V, Bouvet C, Castanié B, Chirol C. Discrete ply modelling of open hole tensile tests. Compos Struct 2014;113:369–81.
[32] Ladevèze P, Lubineau G. On a damage mesomodel for laminates: micro-meso relationships, possibilities and limits. Compos Sci Technol 2001;61 (1):2149–58.
[33] Naik NK, Shembekar PS. Notched strength of fabric laminates I: prediction. Compos Sci Technol 1992;44:1–12.
[34] Kim JK, Kim DS, Takeda N. Notched strength and fracture criterion in fabric composite plates containing a circular hole. J Composite Material 1995;29:982–98.
[35] Xiao J, Bathias C. Damage and fracture of notched non-woven and woven composite laminates. Compos Sci Technol 1994;52(1):99–108.
[36] Belmonte HMS, Manger CIC, Ogin SL, Smith PA, Lewin R. Characterisation and modelling of the notched tensile fracture of woven quasi-isotropic GFRP laminates. Compos Sci Technol 2001;61:585–97.
[37] Afaghi-Khatibi A, Ye L, Mai YW. An effective crack growth model for residual strength evaluation of composite laminates with circular holes. J Compos Mater 1996;30:142–63.
[38] Abisset E, Daghia F, Ladevèze P. On the validation of a damage mesomodel for laminated composites by means of open-hole tensile tests on quasi-isotropic laminates. Compos A Appl Sci Manuf 2011;42(10):1515–24.
[39] Pinho ST. Modelling failure of laminated composites using physically-based failure models [PhD thesis]. Imperial College London; 2005.
[40] Chen BY, Tay TE, Baiz PM, Pinho ST. Numerical analysis of size effects on openhole tensile composite laminates. Compos A Appl Sci Manuf 2013;47:52–62.
[41] Laurin F, Carrere N, Huchette C, Maire J-F. A multiscale hybrid approach for damage and final failure predictions of composite structures. J Compos Mater 2013;47(20–21):2713–47.
[42] Ridha M, Wang CH, Chen BY, Tay TE. Modelling complex progressive failure in notched composite laminates with varying sizes and stacking sequences. Compos A Appl Sci Manuf 2014;58:16–23.
[43] Hallett SR, Green BG, Jiang WG, Wisnom MR. An experimental and numerical investigation into the damage mechanisms in notched composites. Compos A Appl Sci Manuf 2009;40(5):613–24.
[44] Sun XC, Wisnom MR, Halett SR. Interaction of inter- and intralaminar damage in scaled quasi-static indentation tests: Part 2-Numerical simulation. Compos Struct 2016;136:727–42.
[45] Wisnom MR. The role of delamination in failure of fibre-reinforced composites. Philo Transa Royal Soc 2012;370:1850–70.
[46] Bouvet C, Castanié B, Bizeul M, Barrau JJ. Low velocity impact modeling in laminate composite panels with discrete interface elements. Inter J Sol Struct 2009;46(14–15):2809–21.
[47] Ostré B, Bouvet C, Minot C, Aboissière J. Edge impact modeling on stiffened composite structures. Compos Struc 2015;126:314–28.
[48] Lammerant L. Modelling of the interaction between matrix cracks and delaminations during impact of composite plates. Compos Sci Technol 1996;56(10):1171–8.
[49] Aymerich F, Dore F, Priolo P. Prediction of impact-induced delamination in cross-ply composite laminates using cohesive interface elements. Compos Sci Technol 2008;68(12):2383–90.
[50] de Moura MFS, Gonçalves JP. Modelling the interaction between matrix cracking and delamination in carbon-epoxy laminates under low velocity impact. Compos Sci Technol 2004;64(7–8):1021–7.
[51] Laffan MJ, Pinho ST, Robinson P, Iannucci L. Measurement of the in situ ply fracture toughness associated with mode I fibre tensile failure in FRP. Part II: size and lay-up effects. Compos Sci Technol 2010;70(4):614–21.
[52] Pinho ST, Robinson P, Iannucci L. Fracture toughness of the tensile and compressive fibre failure modes in laminated composites. Compos Sci Technol 2006;66(13):2069–79.
[53] Lisle T, Pastor ML, Bouvet C, Margueres P. Damage of woven composite under translaminar cracking tests using infrared thermography. Compos Struct 2017;161:275–86.
[54] Lisle T, Bouvet C, Pastor ML, Margueres P, Prieto Corral R. Damage analysis and fracture toughness evaluation in a thin woven composite laminate under static tension using infrared thermography. Compos Part A 2013;53:75–87.
[55] Raimondo L, Iannucci L, Robinson P, Curtis PT. A progressive failure model for mesh-size-independent FE analysis of composite laminates subject to low-velocity impact damage. Compos Sci Technol 2012;72:624–32.
[56] Bazant ZP, Oh BH. Progressive Crack and band theory for fracture of concrete. Mat Struc 1983;16:155–77.